Earth And Planetary Science Letters
August 2019, Volume 519 Pages 223-233
https://doi.org/10.1016/j.epsl.2019.05.012
https://archimer.ifremer.fr/doc/00767/87880/

On spreading modes and magma supply at slow and ultraslow mid-ocean ridges

Cannat Mathilde [1,*], Sauter Daniel [2], Lavier Luc [3], Bickert Manon [1], Momoh Ekeabino [1], Leroy Sylvie [4]

[1] Marine Geosciences, Institut de Physique du Globe de Paris, UMR 7154 - CNRS, Université de Paris, France
[2] Institut de Physique du Globe de Strasbourg, UMR 7516 - CNRS, Université de Strasbourg, France
[3] Department of Geological Sciences, Institute for Geophysics, Jackson School of Geosciences, The University of Texas at Austin, United States
[4] Sorbonne Université, CNRS-INSU, Institut des Sciences de la Terre de Paris, ISTeP, France

* Corresponding author : Mathilde Cannat, email address : cannat@ipgp.fr

Abstract :

The ultraslow eastern Southwest Indian Ridge (SWIR) offers an opportunity to study the effect of magma supply on an ultraslow mid-ocean ridge starting from quasi-melt-free detachment-dominated spreading, and transitioning to volcanic spreading as one nears prominent axial volcanos. Detachments in the quasi melt-free mode extend along-axis 60 to 95 km and have a lifetime of 0.6 to 1.5 myrs. They cut into their predecessor's footwall with an opposite polarity, causing part of the footwall lithosphere to experience further deformation, hydrothermal alteration, sparse magmatism and possibly thermal rejuvenation, in a hanging wall position. The accretion of the oceanic lithosphere in this context therefore occurs in two distinct stages over the lifetime of two successive detachment faults. We examine the transition from this nearly amagmatic detachment-dominated mode to the more common volcanic mode of spreading, showing that it occurs along-axis over distances <= 30 km. It involves a significant thinning of the axial lithosphere and a gradual decrease of the amount of tectonic displacement on faults, as the magmatic contribution to the divergence of the two plates increases. We develop a conceptual model of this transition, in which magma plays a double role: it fills the space between the diverging plates, thus reducing the need for displacement along faults, and it modifies the thermal state and the rheology of the plate boundary, affecting its thickness and its tectonic response to plate divergence. Based on a comparison of the ultraslow eastern SWIR, with the faster spreading Mid-Atlantic Ridge, we show that the activation of the volcanic, or of the detachment-dominated modes of spreading is connected with the volume of magma supplied per increment of plate separation, over a range of axial lithosphere thickness, and therefore over a range of the M ratio defined by (Buck et al., 2005) as the relative contribution of magma and faults to plate divergence (M is smaller, for a given volume of melt per increment of plate separation, if the plate is thicker). We therefore propose that M does not fully explain the variability in faulting styles observed at slow and ultraslow ridges and propose that rheological changes induced by magma also play a key role (melt itself is weak, hydrothermally altered gabbro-peridotite mixtures are weak, and melt heat sustains more vigorous hydrothermal circulation), resulting in contrasted potentials for strain localization, footwall flexure on faults and the development of detachment faults.

Highlights

► The Southwest Indian Ridge includes corridors of nearly amagmatic spreading. ► New oceanic lithosphere there forms over lifetime of two successive detachment faults. ► Nearly amagmatic corridors transition into more standard magmatic spreading in <30 km. ► Melt supply impacts the thermal state and rheology of the axial lithosphere. ► Melt supply is the main control on spreading mode at slow and ultraslow ridges.

Keywords : slow and ultraslow mid-ocean ridges, divergent plate boundaries, detachment faults, melt supply, axial lithosphere, tectonic and magmatic seafloor spreading processes

1.1 INTRODUCTION

While all mid-ocean ridges are active volcanic chains, slow (<4 cm/yr) and ultraslow (<2 cm/yr) spreading ridges are also rift zones, where normal faults accommodate part of the plate divergence, interacting with magmatism to shape the newly formed oceanic lithosphere. These ridges are segmented, and significant along-axis variations in melt supply accompany this segmentation, with segment ends receiving less magma than the segments centers (Lin et al., 1990). At segment ends, and in whole segments of melt-poor slow and ultraslow ridge regions, large offset normal faults, also called detachment faults, accommodate a large part of the plate divergence (Cann et al., 1997; Cannat et al., 2006; Escartín et al., 2008; Sauter et al., 2013). These detachments bring mantle-derived rocks up through the axial lithosphere, and the resulting seafloor therefore has an ultramafic, non-magmatic component (Cannat, 1993). By contrast, the centers of most slow and ultraslow spreading ridge segments undergo plate divergence through a combination of magma injection and several moderate offset normal faults distributed in the axial domain, and the seafloor exposes volcanic rocks (Smith and Cann, 1999). In the detachment-dominated mode of spreading, specific hydrothermal reactions, associated with the alteration of mantle peridotites, are favored, and feed original microbial communities (Früh-Green et al., 2004). Modes of spreading at slow and ultraslow spreading ridges therefore have a large impact not only on the composition of the oceanic lithosphere, but also on chemical exchanges between the solid Earth and the Ocean, and on the diversity of seafloor biology.

Many questions remain about oceanic accretion in the detachment-dominated mode. What controls the geometry and lifetime of detachments, and how do they root into the mantle? How do hydrothermal and magmatic processes operate in this mode and what are their time and space relations to detachment faulting? What is the architecture of the lithosphere that is accreted in the hanging wall plate? Although it is often assumed to be better constrained, there is also a lot we do not yet know about the volcanic spreading mode at slow and ultraslow ridges. While crustal architecture in this mode is commonly proposed to be similar to the layered magmatic crust formed at fast ridges, there is as yet limited direct evidence in support of this hypothesis, and at least one indication that it might not be the case: while volcanic slow spreading ridge regions have a substantial magma supply, they also have a much thicker (up to 7 km-thick at the Mid-Atlantic Ridge; Wolfe et al., 1995) seismogenic lithosphere, compared with the shallow depth to the axial melt lens of faster ridges (Detrick et al., 1987). Finally, while magma supply is identified as a main control on which of the two spreading modes is activated at slow and ultraslow spreading ridges, and although this control has been tested in numerical models (Behn and Ito, 2008; Buck et al., 2005; Olive et al., 2010; Püthe and Gerya, 2014; Tian and Choi, 2017; Tucholke et al., 2008), there is no clear understanding as yet on how it operates in situ: by what melt supply-related mechanism(s) does a slow spreading ridge switch from the volcanic to the detachment-dominated mode of spreading?

We address several of these questions based on geological, geophysical and petrological data acquired over the course of several cruises in the eastern region of the Southwest Indian Ridge (SWIR; spreading rate of 14 mm/yr; Cannat et al., 2006), east of the Melville Fracture Zone. This 660 km-long ridge region is a low magma supply end-member of the global mid-ocean ridge system (Cannat et al., 2008). It is characterized by a pronounced focusing of the available melt to axial volcanos, separated by corridors of nearly-amagmatic detachment-dominated spreading where the seafloor exposes almost only ultramafic rocks (Cannat et al., 2006; Sauter et al., 2013). Volcanic areas show numerous and mostly spreading-perpendicular scarps and hummocky volcanic ridges, and correspond to more negative gravity anomalies, consistent with seismic crustal thicknesses up to 8 km (Minshull et al., 2006). Nearly amagmatic spreading corridors have, by contrast, a smooth topography, more positive gravity anomalies (Cannat et al., 2006), and a 2 to 5 km-thick seismic crustal layer that is interpreted as made primarily of serpentinized and fractured mantle-derived rocks (Momoh et al., 2017). These rocks are proposed to have been exhumed by successive axial detachment faults, each cutting into the footwall of the previous fault, with an opposite polarity (Sauter et al.,2013). The eastern SWIR therefore offers opportunities to study the links between magma supply and seafloor spreading modes starting from a quasi melt-free regime, and transitioning to volcanic spreading as one nears the axial volcanos.

The formation of many distal continental divergent margins also involves tectonic extension with only incipient magmatism. Specifically, seismic reflectors imaged in the Ocean Continent Transition (OCT) of the Iberian and Australian margins may also have formed by detachment faults that alternated polarity (Gillard et al., 2015; Reston and McDermott, 2011). Divergence rates and melt supply during the OCT phase, and during the following onset of indisputable seafloor spreading at these margins, are not strongly constrained. Our results and hypothesis on the nearly amagmatic seafloor spreading mode, and on its transition to volcanic seafloor spreading at an ultraslow ridge, may nonetheless inform studies of detachment-dominated divergence and mantle exhumation at the OCT phase, and of the transition from OCT to true seafloor spreading.

1. 2 RESULTS

1.2.1 Along-axis extension, and estimated lifetime of successive axial detachments in a nearly amagmatic eastern SWIR spreading corridor

We focus on the nearly amagmatic corridor between the 64°E and 65.6°E axial volcanos (Figure 1). The smooth seafloor there forms 500 to 1000 m-high broad ridges, parallel to the ridge axis, which is nearly orthogonal to the north-south trending direction of plate divergence to the west of 65°E, and up to 25° oblique to the east (Figure 1). Following (Sauter et al., 2013), we interpret these broad ridges (numbered from 1 to 8 going back in time; Figure 1) as formed by successive axial detachments between about 11 myrs-ago (#8) and the present (#1). The along flowline profile in Figure 2 summarizes this tectonic interpretation. Axial detachments #6 (which we propose was initiated about 5.6 myrs ago) to #1 (presently active) each cut into the footwall of the previous detachment, with an opposite polarity (Sauter et al., 2013). Proposed breakaways B7 and B8 are both located in the northern, African plate (Figures 1 and 2) and the corresponding exhumed fault surfaces locally bear spreading-parallel corrugations (Cannat et al., 2009). These two south-facing detachments face volcanic conjugate seafloor in the Australian plate and therefore formed under more magmatically active axial conditions than detachments #6 to #1 (Cannat et al., 2009).

We pick the top of the inward-facing (toward the axis) slope of each ridge as the best approximation (see Appendix Figure A1) for the location of the breakaway of the corresponding detachment fault, and the base of the outward-facing slope of the corresponding broad ridge as the best approximation for the location of the emergence of each fault at the seafloor. The along-axis extension of the eight identified detachments, based on the length of their breakaway (Figure 1 and

Table 1), ranges between 25 km (B7) and 95 km (B4). While these breakaways are mostly straight, the inferred emergence traces show convex-outward undulations, with a typical wavelength of 15-20 km (Figure 1). These likely reflect along-axis changes in the rheology of the detachment footwall, impacting the fault's emergence angle. Most detachment-controlled ridges extend up to, and in the case of B5 (to the west) and B8 (to the west and east), into, adjacent volcanic areas (Figure 1). Breakaway ridges B4, and to a lesser extend B2, in the Antarctic plate, are long and follow the overall trend of the ridge axis, curving from E-W in the west, to ENE-WSW in the east (Figure 1). Breakaway ridges B5 and B7, in the African plate, are shorter and relayed to the east by broad ridges that trend NE-SW, oblique to the N-S spreading direction but parallel to the local trend of the ridge axis. A shorter ENE-WSW ridge, also interpreted as a detachment fault block, is found in an intermediate position to the east of B3 and B5 (Figure 1). These local complexities are interpreted as due to faulting modes specific to oblique nearly amagmatic spreading (Sauter et al., 2013) and are beyond the scope of this paper. We thus focus the following analysis and discussions on the orthogonal-spreading part of the smooth seafloor corridor, to the west of 65°E (Figure 1).

The horizontal offset estimated for past detachments is the along-flowline distance between breakaway and emergence (reconstructed at the time of initiation of the next detachment). For detachment #1, which is still active and at an early stage, the proposed estimate takes mass-wasting into account and is explained in Appendix Figure A1. Estimated horizontal offsets for detachments along the 64.6°E flowline (Figure 2) range between 4 km (active detachment #1; Table 1), and ~21 km (detachments #2 and #8). At a spreading rate of 14 mm/yr (Patriat and Segoufin, 1988), these estimated horizontal offsets correspond to faulting durations (Table 1) between 300 kyrs (detachment #1, still active) and 1.5 myrs (detachment #2) for nearly amagmatic detachments 1 to 6, and of about 2.8 myrs, for corrugated detachments 7 and 8. For nearly amagmatic, flipping polarity detachments # 1 to 6, the horizontal distance between the emergence of a detachment and the location of the next breakaway is 2.8 to 5.6 km (Table 1), indicating that new detachments typically cut into footwall rocks that had been exhumed 200 to 400 kyrs previously.

1.2.2 Footwall to hanging wall: two stages in the generation of melt-starved oceanic lithosphere

A consequence of having successive detachments of opposite polarity that cut into their predecessor's footwall is that the inward-facing slopes of smooth seafloor breakaway ridges are made of material that was initially accreted and transported off-axis as part of the footwall of a detachment fault (Stage 1), then became part of the hanging wall of the next detachment fault (Stage 2). The oceanic lithosphere forming these inward-facing slopes is therefore predicted to have been generated in two stages and over the lifetime of two successive detachment faults.

Stage 2 involves the residence of previously accreted ultramafic seafloor, in the axial valley region as part of the hanging wall of the next axial detachment (Figure 3). Geological observations made in the present-day axial valley near 64.6°E indicate that Stage 2 results in the formation of small offset normal faults and of isolated volcanic patches and ridges, that are distributed in a > 10 km-wide axial valley (Sauter et al., 2013 and Figure 4). Seismic refraction and reflection results obtained in the same area (Momoh et al., 2017) show lower seismic velocities and several sub-horizontal and north-dipping reflectors in the basement of this near-axis domain, consistent with distributed faulting, hydrothermal alteration and magmatic intrusions in the hanging wall of active detachment #1.

The outward-facing slopes of smooth seafloor breakaway ridges record only Stage 1: they form in the footwall of a detachment, and are then captured, and moved off-axis into the footwall of the next (antithetic) detachment. Seafloor ages in the outward-facing slopes of detachment ridges therefore probably increase toward the axis (Figure 3). By contrast, most of the seafloor forming the inward-facing slopes of these ridges has probably been modified by Stage 2 axial valley tectonics, hydrothermal alteration and sparse volcanism, over the lifetime of the next, antithetic detachment. Seafloor spreading in the near absence of melt is therefore predicted to result in complex seafloor age patterns at scales of a few tens of kilometers or less (Figure 3). At larger scales, seafloor ages do nonetheless increase off-axis: pickings for the two best expressed magnetic anomalies in the area (3A and 5; Figure 1) are accordingly consistent with the ages predicted in Table 1 for breakaways B6 and B8.

This two-stage evolution has two predictable consequences, in addition to the generation of a complex lithosphere geology. One is the potential for thermal rejuvenation of the deep lithosphere during Stage 2, as older portions of the footwall of the first detachment find themselves on-axis again in the hanging wall of the next detachment. The other concerns the potential for nearly amagmatic oceanic lithosphere to bear magnetic anomalies. Ultramafic rocks that may have acquired a remanent magnetization upon serpentinization (eg Oufi et al., 2002) in the footwall of the first detachment, would then be subjected to Stage 2 diking and volcanic eruptions in the hanging wall of the next detachment. For example, this could lead to the overprinting of a serpentinization-related magnetic signature recorded up to 2.9 myrs ago at depth in the footwall of detachment #3, by the magnetic signature recorded in volcanic rocks erupted up to 300 kyrs-ago in the hanging wall of detachment #2 (Figure 3). This, in addition to the overall low magnetization of serpentinized peridotites (refs), helps explain why the magnetic anomaly record is poor and ambiguous over the ultramafic seafloor of the study area (Bronner et al., 2014).

1.2.3 Along-axis transition from detachment-dominated to volcanic spreading

Figure 5 shows the transition, in the near-axis region, between nearly amagmatic detachment-dominated spreading (along-flowline profile 1), and more magmatic spreading near the 64°E axial volcano (profiles 3 and 4). Profile 1 has an asymmetrical topography, and the seafloor there exposes almost only serpentinized peridotite (Sauter et al., 2013). Faults in the axial valley floor have vertical offsets <200m; volcanism is sparse, forming isolated ridges and patches, and both rock sampling (Paquet et al., 2016; Sauter et al., 2013) and seismic imaging (Momoh et al., 2017) indicate that magmatic rocks form a volumetrically minor part of the basement. Nearly all the plate divergence is therefore currently accommodated by axial detachment #1. By contrast, profiles 3 and 4, less than 30 km to the west, are located fully within volcanic seafloor, with several volcanic ridges, and fault scarps that have a maximum vertical throw of 1000 m (Figure 5c). The gravity anomalies are in the negative range (Figure 5b), consistent with a thicker crust (Cannat et al., 2006), and we see no evidence in these profiles that detachment #1 is continuing at depths beneath rafted blocks of volcanic seafloor (Reston, 2018; Reston and Ranero, 2012). The axial topography is symmetrical, and seafloor ages from magnetic anomalies (Cannat et al., 2006) increase monotonically with distance to the axis (Figure 5c). These characteristics are consistent with in situ eruption of the volcanics and are typical of seafloor spreading at moderate melt supply, with plate divergence being partitioned into magma emplacement and fault displacement distributed in the axial domain (eg Buck et al., 2005).

Profile 2 is in an intermediate position and cuts the western end of detachment #1 (Figure 5a). The seafloor along this profile shows volcanic morphologies, with spreading perpendicular ridges that are clearly in-situ volcanic constructions (Figure 4 and Sauter et al., 2013), and fault scarps ≤ 200 m-high (Figure 5b); yet the gravity anomalies are in the positive range (Figure 5b). These characteristics are consistent with seafloor spreading at relatively low melt supply, with recent plate divergence being accommodated for a part by detachment #1, and for another part by magma emplacement and smaller offset normal faults distributed in the axial valley. The overall topography of the axial region along profile 2 is distinctly asymmetrical across-axis and similar to that of profile 1. This asymmetric topography is probably mostly due to the broad plate bending effect of the active detachment in the nearly amagmatic eastern domain of profile 1. The axial domain between profiles 2 and 1 is characterized by several volcanic ridges (Figure 4), that formed by local eruptions, on older volcanic seafloor in the west, and directly over ultramafic seafloor to the east (Sauter et al., 2013).

Our near-axis observations therefore point to a gradual transition, over an along-axis distance of less than 30 km, from the detachment-dominated, nearly amagmatic mode of spreading, to a melt-emplacement dominated, symmetrical, mode of spreading. Such a gradual transition indicates that the amount and the distribution of tectonic displacement (one axial detachment, and/or several distributed smaller offset normal faults) at slow spreading ridges are tuned with the melt supply at scales <10 km, so as to complement the melt emplacement contribution to the divergence of the two plates (Figure 6).

1.3 DISCUSSION

1.3.1 Full lithosphere sketches of an ultraslow and magma-poor ridge

Figure 6 illustrates the concept of a gradual transition from the magmatically robust volcanic spreading mode, to nearly amagmatic, detachment-dominated spreading, with tectonic displacement on faults being tuned over the width of the axial domain, to complement melt emplacement so that the two plates diverge at the spreading rate that is imposed by far-field plate tectonics forces. This is similar to the interpretation proposed by (MacLeod et al., 2009) for the along-axis transition from detachment-dominated spreading to more volcanic ridge domains at 13°N on the Mid-Atlantic Ridge (MAR); and an alternative to the rafting detachment model developed by Reston and Ranero (2012) and by Reston (2018), in which axial detachments are proposed to continue at depth beneath rafted blocks of volcanic seafloor at slow and ultraslow ridges. We discard this alternative interpretation because of clear geological evidence that volcanic rocks in the study area were erupted in situ (Figure 4 and recent submersible observations; Cannat et al., AGU abstract 2017).

Figure 6 shows the upper 10 kilometers of the axial domain. Microearthquake depths reported by Schlindwein and Schmid (2016), indicate that the seismogenic lithosphere thickens over an along-axis distance of less than 50 km, from less than 10 km-thick beneath the 65.6°E axial volcano (Figure 1), to about 25 km-thick at the eastern edge of the 64.6°E nearly amagmatic corridor. Assuming that a similar thickening occurs with distance from the 64°E volcano (Figure 1), we infer that the volcanic seafloor at the longitude of profiles 3 and 4, and the nearly amagmatic seafloor at the longitude of profile 1 probably have seismogenic lithosphere thicknesses of about 10-15 km, and 20-25 km, respectively. Transitioning from the two spreading modes therefore also involves thinning the axial seismogenic lithosphere by at least 10 km, over an along-axis distance of ~30 km. In the following paragraphs, we discuss full-lithosphere conceptual sketches based on the present-day geology of the eastern SWIR axis, for the nearly amagmatic and for the volcanic spreading modes.

1.3.1.1 Nearly amagmatic, detachment-dominated spreading mode.

Detachment #1 (Figure 1) presently accommodates nearly all the plate divergence. It cuts through the thick axial brittle lithosphere and roots into ductile shear zones that are documented in dredged ultramafic samples (Bickert et al., AGU abstract, 2018) at the base of the plate (Figure 7a). This detachment is at an early stage (~300 kyrs of activity for a typical detachment lifetime of 1 to 1.5 myrs; Table 1) and has so far caused an estimated maximum footwall flexure of 15° (Appendix Figure A1). This flexure could at least partially be accommodated by reactivation of former detachment #2, accounting for the change of slope observed across the proposed emergence of detachment #2 (E2; Figures 1 and 7a). Sub-horizontal and dipping seismic reflectors documented in the axial valley basement are interpreted as minor conjugate faults and magmatic intrusions in the hanging wall of detachment #1, some of which fed the sparse basalt patches observed at the seafloor (Momoh et al., 2017). These basalts are compositionally distinct from those erupted in the nearby volcanic seafloor domains and, based on their composition, it is unlikely that they erupted from dikes propagating along-axis from these volcanic domains (Paquet et al., 2016). Seafloor imagery (Sauter et al., 2013 and Figure 4) and submersible observations (Cannat et al., AGU abstract, 2017) indicate that most basalt patches are spatially associated with faults that guide melts in the upper levels of the lithosphere (Figure 7a). Melt infiltrations, and dikes intruded at greater depths and presumably for the most part into the footwall plate (Figure 7a) are also documented in peridotites samples from the smooth seafloor domains (Paquet et al., 2016).

Faults and the associated damage also probably channel hydrothermal fluids, so that serpentinization would occur for a good part in and next to the main axial detachment (Andreani et al., 2007; Rouméjon and Cannat, 2014). Sample studies indicate that serpentinization at slow ridges is a multiphase reaction, occurring for the most part in the most kinetically favorable temperature range of 200-350°C, with an initial stage of formation of the serpentine mesh texture at low fluid-rock ratios, followed by several stages of veining and recrystallization of the initial serpentine at higher fluid-rock ratio (Andreani et al., 2007; Früh-Green et al., 2004; Rouméjon et al., 2014). Based on hypocenter depth distribution in melt-poor domains next to the 65.6°E axial volcano, Schlindwein and Schmid (2016) proposed that serpentinization there initiates at depths of ~15 km below seafloor (Figure 7a). Temperatures in the 200-350° C range could, however, also be found at shallower, near seafloor depths in the upflow zone of high temperature, black smoker-type, hydrothermal circulation cells. Such high temperature hydrothermal upflows have not been discovered so far in the area, and given that magmatic rocks are scarce, they should not represent the dominant hydrothermal regime. Yet black smoker-type circulations may develop transiently to cool isolated melt intrusions and trigger episodes of rapid serpentinization in the surrounding ultramafic rocks, both in the footwall and in the hanging wall plates (Figure 7a). Slower, lower temperature serpentinization, as yet not documented by sampling, may also occur in the tectonically damaged footwall and hangingwall domains.

At the current early stage of activity of detachment #1, the axial lithosphere, which we infer formed in the footwall of detachment #2 (Figure 3), is 0.6 to 1.5 myrs-old and could thus be thicker than if controlled solely by the active balance between present-day on-axis heat supply and heat loss. Heat in this spreading mode would be supplied primarily by conduction, by tectonic advection of hot mantle, and by serpentinization reactions. Although advected and latent heat from the sparse melt intrusions could support active black smokers, this efficient mode of hydrothermal cooling would be highly episodic and most hydrothermal circulations would occur at lower fluid-rock ratio in tectonically damaged domains. The resulting axial temperature gradient should therefore be nearly conductive (Figure 7c). Over time and as detachment #1 accommodates more displacement, greater footwall flexure will occur, lowering the fault emergence angle and causing enhanced internal deformation and serpentinization. Also, because of the near-zero melt input, the detachment system should migrate in the direction of the hanging wall and away from the axial region of higher heat input and thinner lithosphere, ultimately favoring the initiation of a new detachment (Buck et al., 2005).

1.3.1.2 More magmatically robust volcanic spreading mode.

The gravity-derived crustal layer on-axis at the longitude of profiles 3 and 4 is 6 to 7 km-thick (Cannat et al., 2006). Plate divergence there thus concerns an axial lithosphere that is thinner than in the nearly amagmatic setting sketched in Figure 7a, but still thicker than the crust. Hence, even if magmatic dikes and gabbro bodies do accommodate most plate divergence in the upper lithosphere, plate divergence acting on the deeper axial lithosphere still requires tectonic uplift of mantle material from the asthenosphere, while through-going melts may form mechanically weak intrusions in this axial lithospheric mantle (Cannat, 1993). Melts intruded higher up will also constitute weak zones while they cool, crystallize, and release the heat necessary to fuel vigorous black smoker-type hydrothermal circulation (eg Lowell et al., 2013). The axial lithosphere in this volcanic setting (Figure 7b) should therefore not just be thinner than in the nearly amagmatic detachment-dominated setting. It should also have a different type of geotherm (Figure 7c), with an upper brittle part that is more efficiently cooled by hydrothermal convection cells, and a lower part that is thinned by frequent melt injections. Temperatures in the upper domain are expected to be variable in space and time (Figure 7c), depending on the activation and geometry of black smoker circulations.

Whether magmatic intrusions that form in the lithospheric mantle are subsequently uplifted into the crust, or remain at deep levels of the new plate as it is transported off-axis, should depend on the distribution and offset of axial faults. In Figure 7b, we propose that several of the symmetrically-distributed axial normal faults observed in profiles 3 and 4 (Figure 5) root into the melt-intruded axial lithospheric mantle, and may thus lift some of its components into the crust: the axial domain of melt emplacement is thinned by faults to produce the off-axis crust. Therefore, although the crustal layer off-axis is probably mostly magmatic, we predict that some magmatic rocks were intruded in the lithospheric mantle, then tectonically uplifted into the crust by successive moderate offset normal faults, together with small volumes of their host mantle rocks. Exhumed mantle-derived rocks have actually been dredged in the volcanic seafloor domain a few km to the north west of profile 4 (Sauter et al., 2013).

This calls for a discussion of the applicability of the popular M ratio concept to this, and to other thick axial lithosphere settings. The M ratio as defined by Buck et al. (2005) is the fraction of the plate divergence accommodated magmatically; (1-M) is accommodated by faults. If melt emplacement by dikes contributes to plate divergence over the full thickness of the brittle axial plate (Buck et al., 2005), M is a direct function of the melt flux (m) per increment of plate separation. On the other hand, M does not directly reflect m if melts are either also emplaced below the plate on-axis (the common case at fast ridges and probably also at magmatically robust slow ridge segments), or if melt emplacement occurs only in a portion of a thick axial brittle plate (probably the common case at ultraslow mid-oceanic ridges). Instead, M then also depends on the thickness of the brittle lithosphere on-axis (H_B), and on the thickness of the domain over which melt can be emplaced (H_M). Olive et al. (2010) addressed this for the $H_M > H_B$ case by defining a second ratio, M_D for the contribution of melt emplaced in the ductile domain. A more generalized approach could be to express m as the cumulated thickness of melt provided per increment of spreading. Most slow and ultraslow settings then have $m < H_B$, and M in this case can be approximated as m/H_B. In the volcanic seafloor configuration of Figure 7b, this yields a M value of ~0.6, for H_B = 12 km and assuming that the off-axis crustal thickness (~7 km) is a good approximation for m (ie that this off-axis crust is mostly free of mantle-derived peridotites, and that there is very little gabbro trapped in the off-axis mantle lithosphere).

1.3.1.3 Transition between the detachment-dominated and volcanic modes of spreading.

Seafloor imagery and sampling (Sauter et al., 2013) suggest that plate divergence at the longitude of profile 2 (Figure 5) occurs by a combination of displacement along the westward continuation of detachment #1, along smaller offset normal faults in the axial valley, and by magmatic injections forming spreading-perpendicular volcanic ridges (Figure 4). As a result, the geophysically-defined crustal layer should be more geologically composite than in the nearly amagmatic smooth seafloor configuration (Figure 7a), with proportions of serpentinized ultramafic rocks and magmatic intrusions that would depend both of recent magmatic input, and of whether the axial configuration in the recent past was more magmatic (in which case the crust offset by detachment #1 would be mostly magmatic), less magmatic (in which case this crust would be mostly ultramafic) or similarly magmatic.

Compared to the nearly amagmatic configuration, more melts would transit through and react with the lower lithospheric axial mantle. These deep melts would slowly release their heat into the surrounding mantle and would therefore keep the lower axial lithosphere thinner and hotter than in Figure 7a. A further increase in the melt supply would eventually allow for axial faults (and for the hydrothermal systems that develop in permeable brittle rocks) to reach down to very near these melt-rich and hot regions, leading to vigorous hydrothermal circulation. This configuration would ultimately resemble the more magmatically robust volcanic mode of Figure 7b. The effect of melts emplaced in thick lithosphere, ultraslow spreading ridge settings thus goes beyond the mere mechanical accommodation of plate divergence. Melts thin and weaken the lithosphere (thereby modifying the thickness and strength of the rigid domain in which plate separation needs to be accommodated). Melts emplaced in the brittle lithosphere also modify the axial thermal regime by fueling vigorous, if transient, hydrothermal circulation. We propose that these combined effects (rheological and thermal) are key to understand how the two highly contrasted ridge settings proposed in Figure 7, transition along-axis over distances <30 km.

1.3.2 Spreading rate, melt supply, and the spreading mode at slow and ultraslow ridges

Spreading rate has a large impact on the thermal regime of mid-ocean ridges (eg Chen and Morgan, 1990). With a spreading rate about half of that of the MAR, the SWIR is expected to have a thicker axial lithosphere in places where the melt budget per unit of plate separation is the same, and a fortiori also in places where this melt budget is less (the axial lithosphere should be even thicker due to a lesser input of magmatic heat). At a given melt supply, lithosphere thickness affects the fraction (M; Buck et al., 2005) of the plate divergence that is accommodated magmatically. It could therefore have an effect on the spreading mode. We now assess this effect through a comparison of well-studied axial configurations at the MAR and SWIR.

The nearly amagmatic flip-flop detachment (after the terminology of Reston and McDermott, 2011) mode documented at the ultraslow SWIR has not so far been identified at slow ridges, an absence that probably results from more extreme degrees of along-axis melt focusing at ultraslow ridges, another consequence of having a very thick axial lithosphere (Cannat et al., 2003; Standish et al., 2008). The other two modes of slow spreading accretion (volcanic and corrugated detachment modes) are common to both slow and ultraslow settings and therefore offer points of comparison. Microseismicity results acquired at 13°N at the Mid-Atlantic Ridge, and in the 49°E region of the SWIR indicate seismogenic lithosphere thicknesses of up to 15 km and 20 km respectively (Parnell-Turner et al., 2017; Yu et al., 2018). Corrugated core-complexes that form in the Antarctic plate at 49°39'E on the SWIR (Zhao et al., 2013), therefore result from detachments that cut through some 20 km of brittle lithosphere, compared to up to 15 km for the 13°N MAR detachments (Figure 8). There is no evidence for a significant contrast between the two settings in terms of the volume of melt supplied per increment of plate separation: in the two cases, exposed detachment surfaces face volcanic seafloor in the other plate (MacLeod et al., 2009; Zhao et al., 2013); and seismic crustal thicknesses are similar (within a 2-5 km range in the two settings). Along the same line, the volcanic axial configuration in profiles 3 and 4 of Figure 4 resembles that observed at MAR segment centers, with a symmetrical topography, distributed faults and a crustal thickness of 6-7 km, yet it has an axial seismogenic plate thickness that is probably greater (10 to 15 km; Schlindwein and Schmid, 2016) than documented for volcanic domains of the MAR (less than 8 km; Wolfe et al., 1995), and more similar to that of corrugated detachment MAR domains (Figure 8).

These comparisons therefore suggest that the activation of the volcanic, or of the corrugated mode of spreading at slow and ultraslow ridges is connected more to the volume of melt per increment of plate separation, than to the thickness of the axial lithosphere. The relative contribution of magma and faults to plate divergence, expressed as the M ratio (Buck et al., 2005), is less, for a given magmatic contribution, if the axial brittle plate is thicker. The volcanic and corrugated modes therefore both appear to be activated at lower M at ultraslow than at slow ridges. The explanation we now explore is that the impact of the axial lithosphere on spreading modes at slow and ultraslow ridges lies not just in its actual thickness, but also in its strength, and that this strength is affected by melt supply.

Detachment-dominated modes, corrugated or not, develop for substantial lithosphere thicknesses (Figure 8). MAR corrugated detachments are steep at depth (ca 70°; de Martin et al., 2007; Parnell-Turner et al., 2017) but, when mature, emerge at the seafloor at very low angles (<15°; Smith et al., 2006), indicating low footwall flexural rigidity. Smooth seafloor detachments in nearly amagmatic corridors of the SWIR experience substantial, althought probably not as large, footwall flexure (Momoh et al., EGU abstract, 2019). Given that the axial lithosphere is not thin in either case, such large flexures call for mechanisms that weaken the detachment footwall as faulting proceeds, forming weaker domains in an otherwise thick mechanical lithosphere (Buck, 1988; Lavier et al., 1999). Most slow spreading ridge numerical models to date have implemented this effect by making rock strength a function of strain (Lavier et al., 1999). Geological ground truth comes from studies of samples from the exposed footwall of axial detachments. These studies show that strain localization occurs primarily in assemblages of one or several weak hydrous minerals (serpentine, chlorite, amphibole and talc; Boschi et al., 2006; Escartín et al., 2003; Picazo et al., 2012; Schroeder and John, 2004) that form in the hydrothermally altered brittle lithosphere, at greenschists facies temperatures (<500°C). Talc, specifically, is significantly weaker than serpentine, and is not formed in substantial amounts from peridotites without the input of additional silica, via metasomatic hydrothermal fluids that have altered magmatic rocks, or directly from magmatic veins intruded in the peridotites (Boschi et al., 2006; Picazo et al., 2012). Talc is uncommon in samples from the nearly amagmatic smooth seafloor (Rouméjon et al., 2014). It is by contrast common in samples from corrugated seafloor. Large footwall flexure in the corrugated detachment mode is therefore likely facilitated by talc forming from peridotite gabbro mixtures, while nearly amagmatic detachments would operate with more rigid footwalls (Cannat et al., 2009). Higher melt supply, leading to a transition from the corrugated detachment to the volcanic mode, would also likely strengthen the brittle lithosphere (Cannat et al., 2009) because: 1- the proportion of mantle-derived peridotites would become too small to form pervasive serpentine and or talc-bearing zones of weakness; and 2- new magmatic intrusions, which initially form weak melt-mush and ductile gabbro, turn, as they cool, into pristine and strong brittle magmatic rocks (Figure 8). More abundant melt, by contrast, weakens the ductile axial lithosphere. The nearly amagmatic detachment mode is therefore expected to be distinct from both the corrugated detachment, and the volcanic mode, in that it operates with a significantly stronger lower axial lithosphere (Figure 8), which should oppose flexure and prevent the development of detachments (Lavier, 2002). Field evidence that detachments exist in the SWIR nearly amagmatic spreading corridors therefore indicates that additional strain weakening mechanisms are activated in this context. Microstructures in ductile and semi-brittle shear zones in dredged ultramafic samples show that dynamic grain size reduction in the ductile mantle lithosphere is a plausible candidate (Bickert et al., AGU abstract, 2018).

1.4 CONCLUSIONS

We propose the following conclusions:

1- new oceanic lithosphere in the nearly amagmatic detachment-dominated mode is accreted over the lifetime of two successive detachment faults (ie over 1.5 to 3 myrs) and is for the most part made of material that experienced a two-stages tectonic, hydrothermal, and magmatic evolution: first in the footwall of one detachment fault, then in the hanging wall of the next detachment fault.

2- individual active detachments extend over the whole along-axis width of nearly amagmatic seafloor spreading corridors, up to 95 km in the case studied here. They accommodate up to 20 km of plate divergence, and probably cut through a very thick axial lithosphere (≥25 km). Breakaways are straight, cutting into ultramafic seafloor that was exhumed up to 400 kyrs previously in the former detachment fault's footwall. The emergence of mature detachment faults shows 15-20 km-long undulations, which we propose are due to along-axis changes in the rheology of the detachment footwall, impacting the fault's emergence angle.

3- the along-axis transition from nearly amagmatic, detachment-dominated spreading, to more magmatic spreading next to axial volcanic centers, occurs gradually over distances of < 30 km through a fine tuning of tectonic displacement on faults to the local rates of melt emplacement, so as to accommodate the plate divergence. We propose that this gradual transition involves two main processes that are both related to the increase of melt supply: 1- more melt reduces the need for displacement on faults as a mean to accommodate plate divergence; 2- more melt heats and weakens the deep axial lithosphere, thus reducing the thickness of the rigid domain over which divergence needs to be accommodated.

4- A comparison with the slow spreading MAR further suggests that the activation of the volcanic or detachment-dominated modes of spreading at slow and ultraslow spreading ridges is primarily controlled by the melt budget (the volume of melt supplied per unit of plate separation), over a range of axial lithosphere thickness (the thickness of the plate over which divergence must be accommodated, decreasing with spreading rate at a given melt budget). Spreading modes are therefore not determined solely by the relative contribution of magma and faults to plate divergence (the M ratio of Buck et al., 2005), since this relative contribution also depends on axial lithosphere thickness . We propose that the rheology of the axial lithosphere is a key additional parameter, that is also affected by the melt supply. Melt heat can sustain vigourous, black smoker type hydrothermal circulations that impact the thermal state of the lithosphere and favor enhanced hydrothermal alteration. Melt, magmatic rocks, and hydrothermally altered gabbro-peridotite mixtures, also modify the strength of the brittle lithosphere, resulting in contrasted potentials for strain localization and footwall flexure, the strongest configuration being that of the most magmatically robust (volcanic) mode, and the weakest and most favorable to long-lasting detachments and large flexure, being that of the moderately magmatic (corrugated) detachment mode. Finally, the presence of melt weakens the ductile mantle at the base of the brittle plate, so that the nearly amagmatic detachment mode probably operates on axial domains that are characterized by a strong ductile lithospheric mantle that is lacking in the more magmatic corrugated detachment and volcanic modes of spreading.

Acknowledgements:

We thank Garrett Ito and Taras Gerya, our two reviewers, for their comments and suggestions. We acknowledge partial funding by CNRS-INSU post cruise research grants obtained in 2015 and 2017 and by ANR project "Ridge-Factory-Slow". This is IPGP paper #4025.

APPENDIX

Mapping of axial detachment faults and estimating their age and lifetime in melt-poor oceanic lithosphere

In order to map past detachment faults in the nearly amagmatic spreading corridor of Figure 1, and to estimate their age and lifetime (Table 1), we picked the top of the inward-facing (toward the axis) slope of each detachment-controlled ridge as the best approximation for the breakaway, and the base of their outward-facing slope as the best approximation for the emergence. This approach yields uncertainties, primarily due to the effect of landslides, as illustrated in Figure A1 for presently active detachment #1. For young detachments, the (eroded) breakaways (B in Figure A1) may be a few hundred meters closer to the ridge axis than the top of the inward-facing slope of the detachment ridge, but this discrepancy should diminish and eventually disappear as flexure proceeds so that the outward facing slope of the detachment ridge steepens and also gets subjected to landslides (Figure A1f). Similarly, the emergence of an active detachment may be several hundred meters closer to the breakaway than the base of the detachment-controlled axial relief, which may correspond instead to the front of landslide deposits (Figure A1d). For past detachments, however, this domain has been captured into the footwall of a more recent detachment, probably causing flexure-related deformation and further obscuring the relation between the base of the slope and the past location of the emergence. We estimate that picking the emergence of past detachments at the base of the outward-facing slopes is the most straightforward approach, although it may introduce errors of up to 2 km / 142 kyrs in the estimated displacement/duration of individual detachments. This is a large error on individual detachments. However, because seafloor spreading in the study area has almost fully been accommodated by detachment faulting from the initiation of detachment #6 (6.1 myrs ago; Table 1), to the present, individual errors made with our method on each detachment must be compensated on the others, within 2 km.

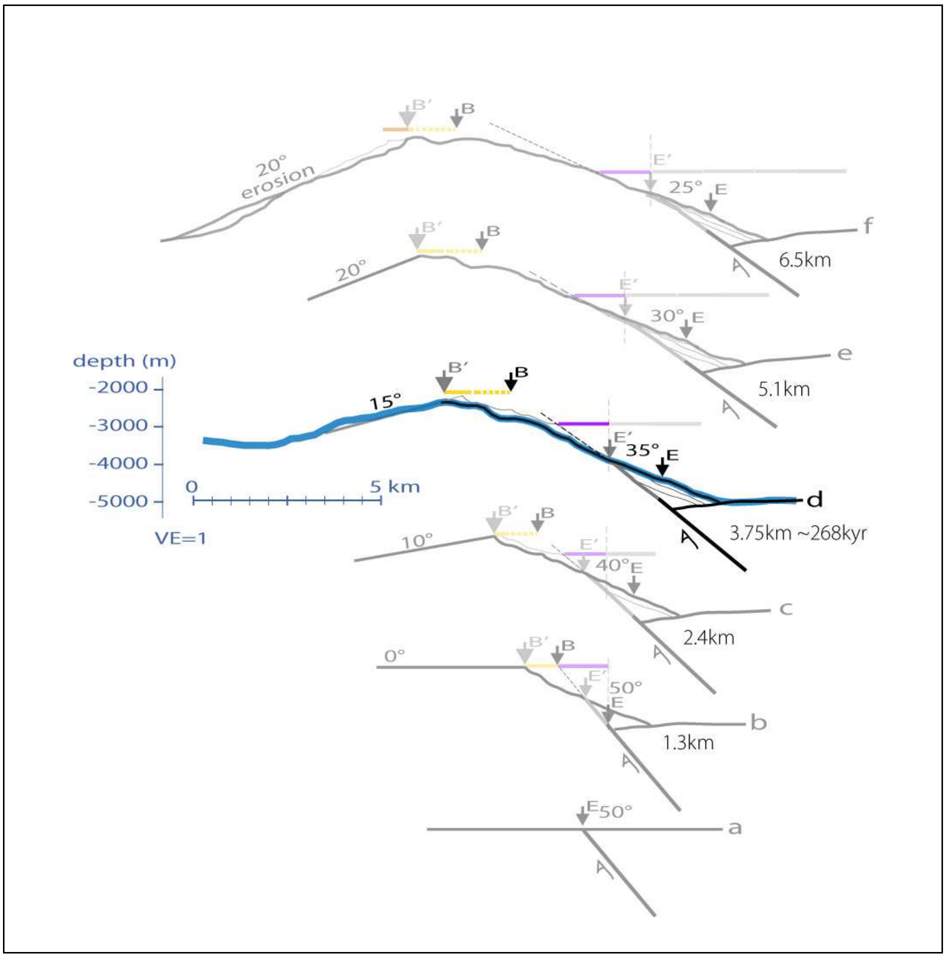

Figure A1. Conceptual sketches illustrating the possible evolution of presently active detachment #1. This detachment is at an early stage. Its proposed present-day configuration is shown in A1d, with the measured axial bathymetric profile in blue (no vertical exaggeration). The dip (~35°) and location of the emergence are based on recent submersible observations (Cannat et al., AGU abstract 2017). Panels A1c to A1a are back in time, and panels A1e to A1f into the near future, assuming a progressive footwall flexure, resulting in a decrease of the faults emergence angle from an initial 50° dip (although not shown, we assume that fault dips also increase with depth); and a 20° slope stability angle for serpentinites (Cannat et al., 2013), which is maintained at each step by landslides so that the eroded cross sectionnal area equals that of landslide deposits. In the natural case, slope failure may be differed to after a significant unstable relief is constructed. B is the location of the actual breakaway, and B' is the location of the top of the ridge-ward slope at each step. The distance between B and B' results from mass-wasting and is expected to decrease with increasing offset and flexure along the detachment. E is the emergence of the fault with respect to the hanging wall plate, and E' is the emergence from the landslide package. Based on this sketch, our best estimate for the horizontal offset/duration of detachment #1 are about 4 km/300 kyrs (Table 1).

detachment #	facing	along-axis extension at breakaway km	horizontal distance from emergence to breakaway km (±0.5)	horizontal distance from emergence to breakaway of next detachment km (±0.5)	Estimated total plate divergence km	estimated fault duration myr	age of breakaway myr	age of seafloor at breakaway myr
1 (active)	south	85	*(4)*		*(4)*	*(0.3)*	*(0.3)*	*(0.6)*
2	north	75	21	4.2	21	1.5	1.8	2.2
3	south	60	16.2	5.6	16	1.1	2.9	3.1
4	north	95	14	2.8	14	1	3.9	4.3
5	south	60	15.1	4.7	15	1.1	5	5.2
6	north	60	9.3	3.2	9	0.6	5.6	6.1
7 (corrugated)	south	25	19.5	6.3	*(39)*	*(2.8)*	8.4	8.4
8 (corrugated)	south	45	20.6		*(41)*	*(2.9)*	*(11.3)*	*(11.3)*

TABLE 1. Characteristics of successive axial detachments as measured and estimated (see Appendix) along the profile of Figure 2.

FIGURE CAPTIONS

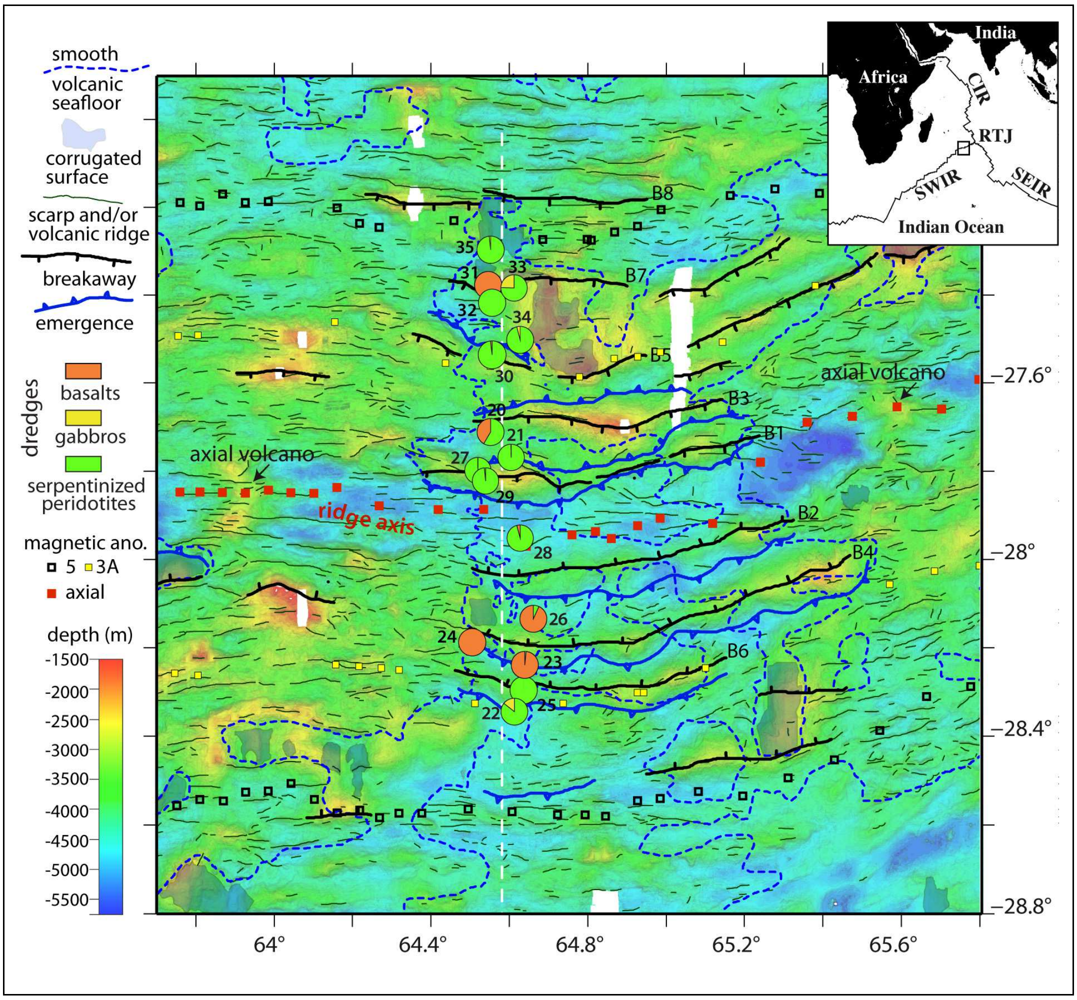

Figure 1. Tectonic sketch map showing the proposed breakaways and emergences of successive detachments in the 64.6°E nearly amagmatic corridor; the volcanic scarps and ridges in the more magmatically active volcanic domains to the east and west; the contours of these volcanic domains, and of several corrugated detachment surfaces and pickings for magnetic anomalies 0, 3A and 5 (Cannat et al., 2006); the recovered lithologies in 16 dredges (Sauter et al., 2013); and the location of the cross-section shown in Figure 2. Detachment faults breakaways (B) and emergences are numbered from 1 (presently active) to 8 (initiated at the time of magnetic anomaly 5; ~11 Myrs ago).

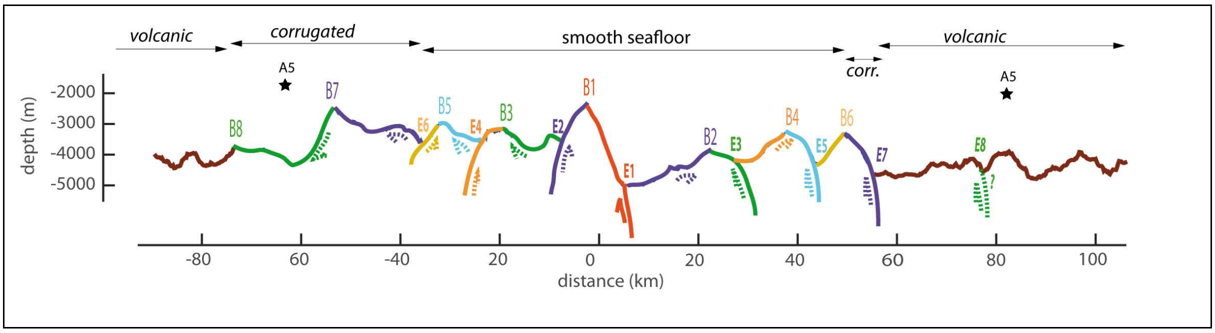

Figure 2. Tectonic interpretation of the along flowline cross-section located in Figure 1, modified after (Sauter et al., 2013), showing the proposed sequence of successive detachments leading to the continuous exposure of ultramafic rocks in the two diverging plates in smooth seafloor domain (detachments #6 to 1), or in the northern, African plate, facing volcanic seafloor in the Antarctic plate (corrugated-volcanic seafloor domains; detachments #8 and 7). Stars: pickings of anomaly A5 in nearest shipboard magnetic profile (Cannat et al., 2006).

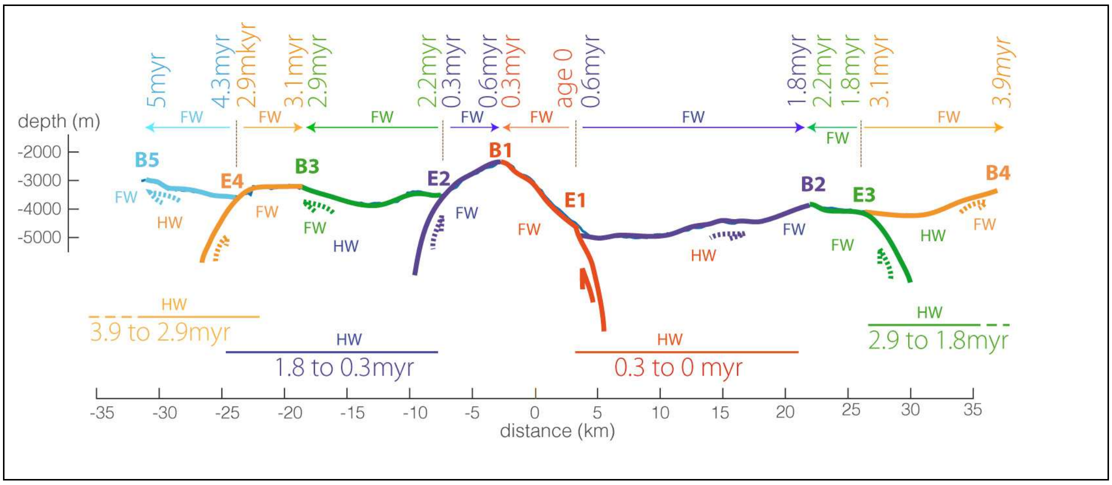

Figure 3. Tectonic interpretation of the along flowline cross-section located in Figure 1. Zoom to the near-ridge region, showing the ages estimated (text and Table 1) for the initial exposure of ultramafic rocks in the footwall (FW) of each detachment, and for subsequent tectonics, incipient volcanism, and hydrothermal alteration in the hanging wall (HW) of the next detachment.

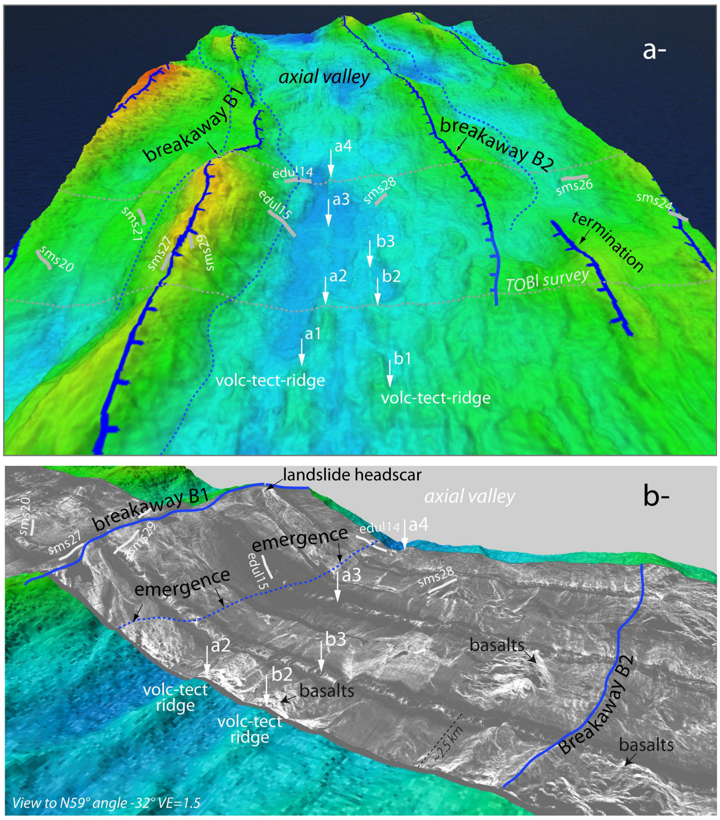

Figure 4. Perpective views of the near axis region in the 64.6°E nearly amagmatic corridor. a- bathymetry (depth scale as in Figure 1) with proposed detachment fault breakaways B1 and B2, dredge tracks (in grey, recovered rocks are > 90% ultramafic; (Sauter et al., 2013)), and outlines of the TOBI (Towed Ocean Bottom Instrument) survey (Sauter et al., 2013). b- TOBI reflectivity image drapped on bathymetry. Hummocky basaltic outcrops rest on less reflective ultramafic seafloor. They tend to form spreading-perpendicular ridges (a1-a2 and b1-b2), that align with small offset faults of the ultramafic basement (a2 to a4 and b2 to b3; these faults are more visible in the bathymetry of panel a). The location of the emergence of detachment #1 is based on recent submersible observations (Cannat et al., AGU abstract 2017).

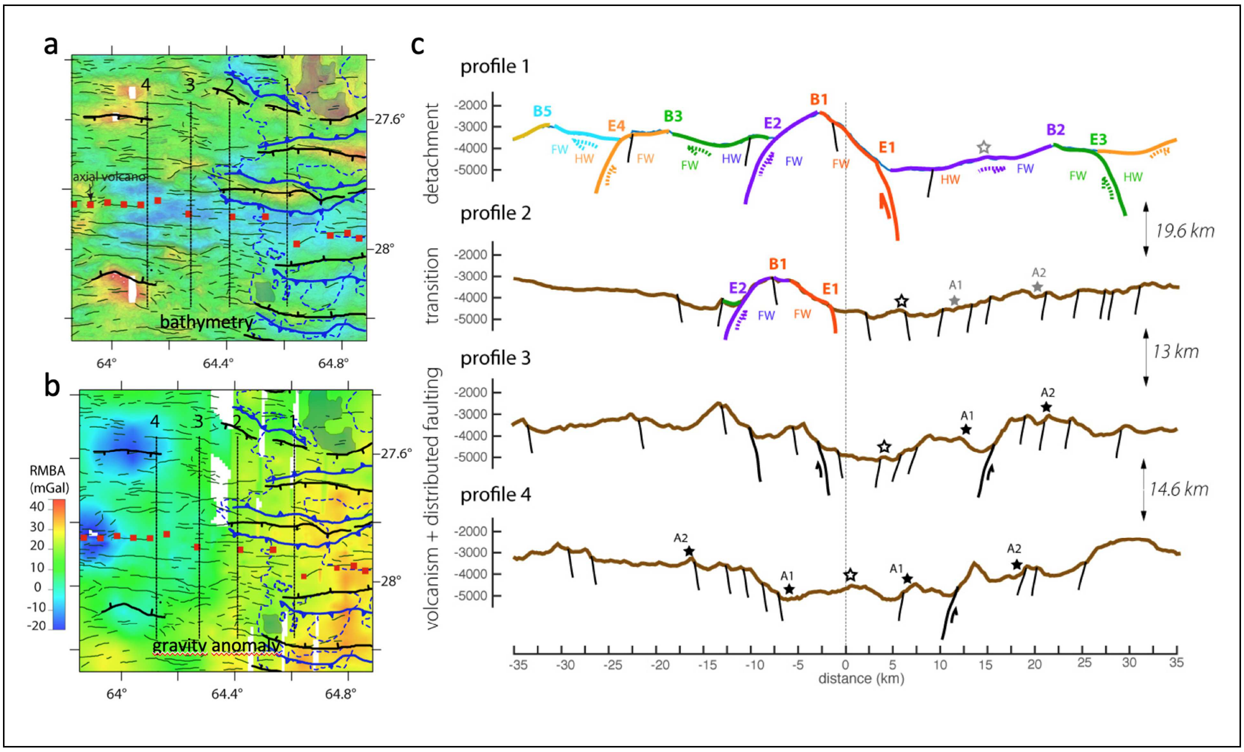

Figure 5. Tectonic interpretation of 4 along flowline cross-sections distributed over the transition from nearly amagmatic seafloor in the east (profile 1), to fully volcanic seafloor in the west (profiles 3 and 4). Panels a and b show the location of these profiles on bathymetry (depth scale, tectonic features and axial magnetic anomaly pickings as in Figure 1) and on a residual mantle Bouguer anomaly map (Cannat et al., 2006). Panel c: seafloor is colored as in Figure 2 for ultramafic seafloor, and in brown for volcanic seafloor; magnetic anomalies 0 (open star), A1 and A2 (closed stars, grey when picking is ambiguous) as in (Cannat et al., 2006).

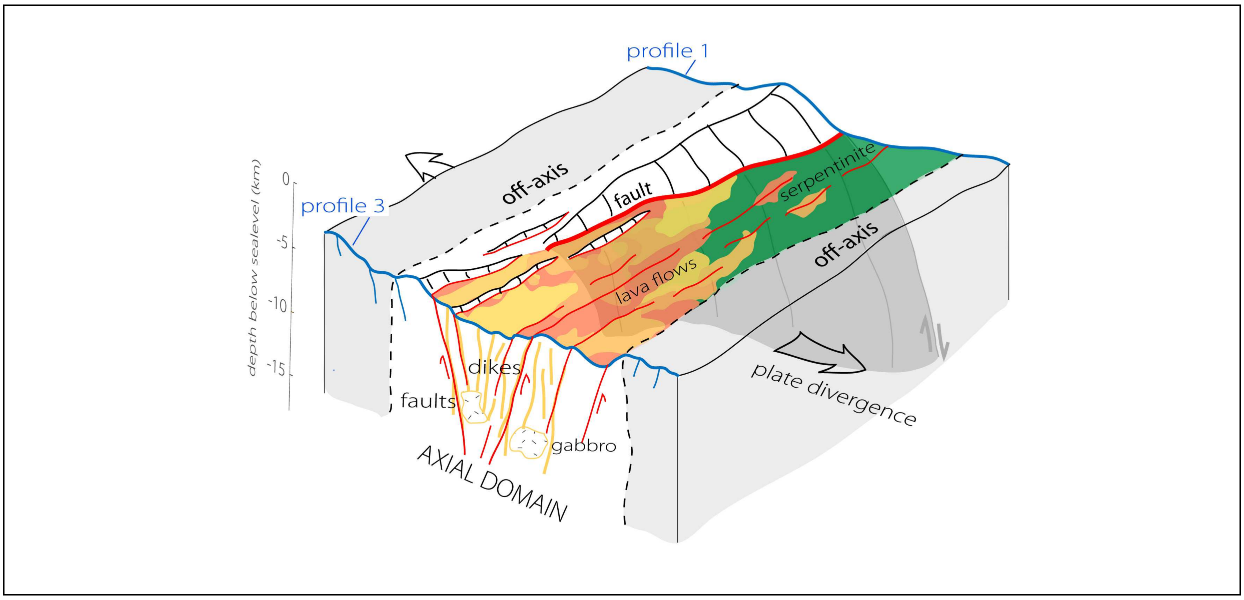

Figure 6. 3D perspective sketch of the axial region between across-axis profiles 1 and 3 (in blue; location and tectonic interpretation of these profiles in Figure 5). The concept illustrated here is that tectono-magmatic processes that accommodate plate divergence are tuned so that along-axis variations of melt supply are compensated by greater tectonic displacement on faults. In the nearly amagmatic configuration of profile 1, most plate divergence occurs at a single detachment fault, while in the more magmatically active configuration of profile 3, only 30 km away along-axis, the same total amount of divergence occurs through distributed faulting and magmatic injections. This sketch only goes down ~10 km into basement and therefore does not fully reach to the base of the lithosphere, particularly in the nearly amagmatic configuration, where it probably is >25km-deep (Schlindwein and Schmid, 2016). Full plate 2D sketches for the configurations of profiles 1 and 3 are shown in Figure 7.

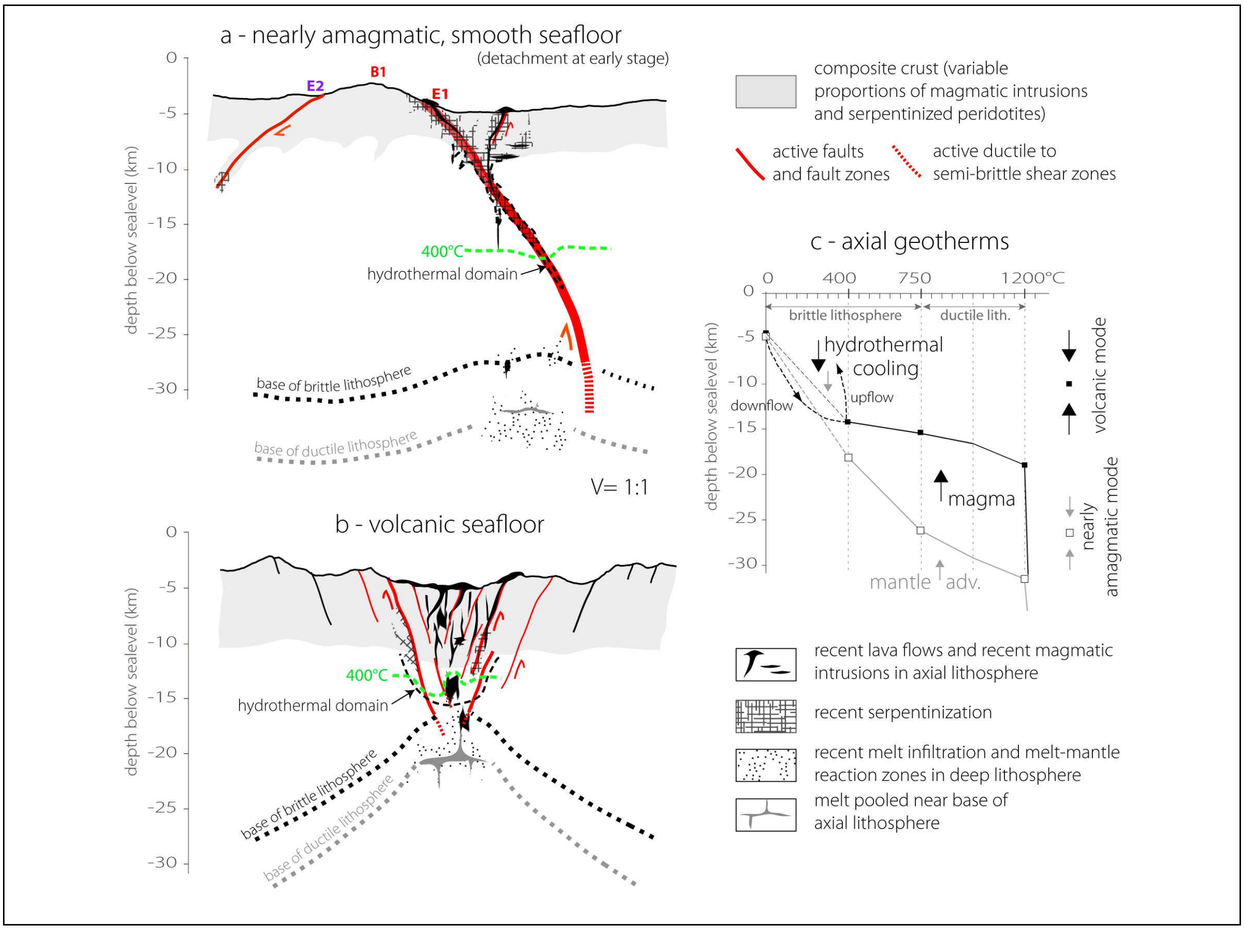

Figure 7. No vertical exaggeration, full plate 2D conceptual sketches of the ridge axis (a and b) and of axial geotherms (c) for across-axis profiles 1 and 3 (location in Figure 5). The base of the brittle lithosphere in a and b is drawn from constraints on the depth of seismicity (Schlindwein and Schmid, 2016). The crust (grey) is a low density, low seismic velocity layer. It is sketched on the basis of gravity and seismic velocity constraints (Cannat et al., 2006; Momoh et al., 2017), and formed by the combination of magmatic flows, intrusions, fault damage, and serpentinization. For clarity, the axial sketches only show the most recent magmatic flows, intrusions, and infiltrations, and the most recently serpentinized domains. See text (subsection 1.3.1) for explanations.

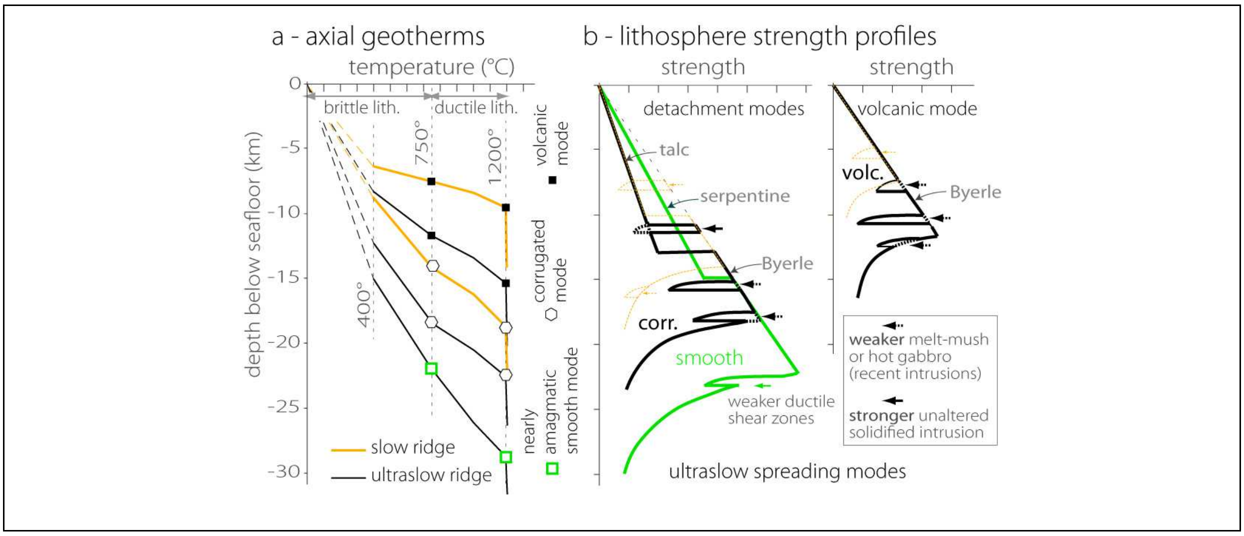

Figure 8. Conceptual sketches of axial geotherms (a) and lithosphere strength profiles (b) for the nearly amagmatic smooth seafloor detachment mode, the weakly magmatic corrugated detachment mode, and the magmatically more robust volcanic spreading mode, at slow and ultraslow ridges. Depth to the base of the brittle lithosphere is based on constraints on the depth of seismicity at the MAR and SWIR (Parnell-Turner et al., 2017; Schlindwein and Schmid, 2016; Wolfe et al., 1995; Yu et al., 2018). Thermal gradients in the lower lithosphere are inferred to be higher at higher melt supply (see Figure 7c and text). Lithosphere strength (not scaled) is a function both of lithosphere thickness, and of two types of weakening mechanisms: hydrothermal alteration yielding weaker minerals (simplified here as a choice between serpentine or mechanically weaker talc; see text subsection 1.3.2); and melt injection, which initially weakens the plate as the melt cools, then could make it locally stronger (if cutting though weak, hydrothermally altered exhumed mantle). These weakening mechanisms differ between the 3 spreading modes and are proposed to contribute to the transition from one mode to another at varying melt supply (see text subsection 1.3.2).

REFERENCES

Andreani, M., Mével, C., Boullier, A.M., Escartín, J., 2007. Dynamic control on serpentine crystallization in veins: Constraints on hydration processes in oceanic peridotites. Geochemistry, Geophysics, Geosystems 8. https://doi.org/10.1029/2006GC001373

Behn, M.D., Ito, G., 2008. Magmatic and tectonic extension at mid-ocean ridges: 1. Controls on fault characteristics. Geochemistry, Geophysics, Geosystems 9. https://doi.org/10.1029/2008GC001965

Boschi, C., Früh-Green, G.L., Escartín, J., 2006. Occurrence and significance of serpentinite-hosted, talc- and amphibole-rich fault rocks in modern oceanic settings and ophiolite complexes: An overview. Ofioliti 31, 129–140. https://doi.org/10.4454/ofioliti.v31i2.335

Bronner, A., Sauter, D., Munschy, M., Carlut, J., Searle, R., Cannat, M., Manatschal, G., 2014. Magnetic signature of large exhumed mantle domains of the Southwest Indian Ridge – Results from a deep-tow geophysical survey over 0 to 11 Ma old seafloor. Solid Earth 5, 339–354. https://doi.org/10.5194/se-5-339-2014

Buck, W.R., 1988. Flexural rotation of normal faults. Tectonics. https://doi.org/10.1029/TC007i005p00959

Buck, W.R., Lavier, L.L., Poliakov, A.N.B., 2005. Modes of faulting at mid-ocean ridges. Nature 434, 719–723. https://doi.org/10.1038/nature03358

Cann, J.R., Blackman, D.K., Smith, D.K., McAllister, E., Janssen, B., Mello, S., Avgerinos, E., Pascoe, A.R., Escartin, J., 1997. Corrugated slip surfaces formed at ridge-transform intersections on the Mid-Atlantic Ridge. Nature 385, 329–332. https://doi.org/10.1038/385329a0

Cannat, M., 1993. Emplacement of mantle rocks in the seafloor at mid-ocean ridges. Journal of Geophysical Research 98, 4163–4172. https://doi.org/10.1029/92JB02221

Cannat, M., Céline, R.J., Fujimoto, H., 2003. Melt supply variations to a magma-poor ultra-slow spreading ridge (Southwest Indian Ridge 61° to 69°E). Geochemistry, Geophysics, Geosystems 4, 1–21. https://doi.org/10.1029/2002GC000480

Cannat, M., Mangeney, A., Ondréas, H., Fouquet, Y., Normand, A., 2013. High-resolution bathymetry reveals contrasting landslide activity shaping the walls of the Mid-Atlantic Ridge axial valley.

Geochemistry, Geophysics, Geosystems 14, 996–1011. https://doi.org/10.1002/ggge.20056

Cannat, M., Sauter, D., Bezos, A., Meyzen, C., Humler, E., Le Rigoleur, M., 2008. Spreading rate, spreading obliquity, and melt supply at the ultraslow spreading Southwest Indian Ridge. Geochemistry, Geophysics, Geosystems. https://doi.org/10.1029/2007GC001676

Cannat, M., Sauter, D., Escartín, J., Lavier, L., Picazo, S., 2009. Oceanic corrugated surfaces and the strength of the axial lithosphere at slow spreading ridges. Earth and Planetary Science Letters 288, 174–183. https://doi.org/10.1016/j.epsl.2009.09.020

Cannat, M., Sauter, D., Mendel, V., Ruellan, E., Okino, K., Escartin, J., Combier, V., Baala, M., 2006. Modes of seafloor generation at a melt-poor ultraslow-spreading ridge. Geology 34, 605–608. https://doi.org/10.1130/G22486.1

Chen, Y., Morgan, W.J., 1990. A Nonlinear Rheology Model for Mid-Ocean Ridge Axis Topography The relative size of the decoupling chamber to the size lated to form the theory for the oceanic of the plastic failure zone within the brittle plate determines the sphere and an iteration sch. Journal of Geophysical Research: Solid Earth 95.

de Martin, B.J., Reves-Sohn, R.A., Canales, J.P., Humphris, S.E., 2007. Kinematics and geometry of active detachment faulting beneath the Trans-Atlantic geotraverse (TAG) hydrothermal field on the Mid-Atlantic Ridge. Geology 35, 711–714. https://doi.org/10.1130/G23718A.1

Detrick, R.S., Buhl, P., Vera, E., Mutter, J., Orcutt, J., Madsen, J., Brocher, T., 1987. Multi-channel seismic imaging of a crustal magma chamber along the East Pacific Rise. Nature. https://doi.org/10.1038/326035a0

Escartín, J., Mével, C., MacLeod, C.J., McCaig, A.M., 2003. Constraints on deformation conditions and the origin of oceanic detachments: The Mid-Atlantic Ridge core complex at 15°45′N. Geochemistry, Geophysics, Geosystems. https://doi.org/10.1029/2002GC000472

Escartín, J., Smith, D.K., Cann, J., Schouten, H., Langmuir, C.H., Escrig, S., 2008. Central role of detachment faults in accretion of slow-spreading oceanic lithosphere. Nature 455, 790–794. https://doi.org/10.1038/nature07333

Früh-Green, G.L., Connolly, J.A.D., Plas, A., Kelley, D.S., Grobéty, B., 2004. Serpentinization of oceanic peridotites: Implications for geochemical cycles and biological activity. Geophysical Monograph Series 144, 119–136. https://doi.org/10.1029/144GM08

Gillard, M., Autin, J., Manatschal, G., Sauter, D., Munschy, M., Schaming, M., 2015. Tectonomagmatic evolution of the final stages of rifting along the deep conjugate Australian-Antarctic magma-poor rifted margins: Constraints from seismic observations. Tectonics. https://doi.org/10.1002/2015TC003850

Lavier, L.L., 2002. Half graben versus large-offset low-angle normal fault: Importance of keeping cool during normal faulting. Journal of Geophysical Research 107, 2122. https://doi.org/10.1029/2001JB000513

Lavier, L.L., Buck, W.R., Poliakov, A.N.B., 1999. Self-consistent rolling-hinge model for the evolution of large-offset low-angle normal faults. Geology 27, 1127–1130. https://doi.org/10.1130/0091-7613(1999)027<1127:SCRHMF>2.3.CO;2

Lin, J., Purdy, G.M., Schouten, H., Sempere, J.C., Zervas, C., 1990. Evidence from gravity data for focused magmatic accretion along the Mid-Atlantic Ridge. Nature. https://doi.org/10.1038/344627a0

Lowell, R.P., Farough, A., Hoover, J., Cummings, K., 2013. Characteristics of magma-driven hydrothermal systems at oceanic spreading centers. Geochemistry, Geophysics, Geosystems 14, 1756–1770. https://doi.org/10.1002/ggge.20109

MacLeod, C.J., Searle, R.C., Murton, B.J., Casey, J.F., Mallows, C., Unsworth, S.C., Achenbach, K.L., Harris, M., 2009. Life cycle of oceanic core complexes. Earth and Planetary Science Letters 287, 333–344. https://doi.org/10.1016/j.epsl.2009.08.016

Minshull, T.A., Muller, M.R., White, R.S., 2006. Crustal structure of the Southwest Indian Ridge at 66°E: Seismic constraints. Geophysical Journal International 166, 135–147. https://doi.org/10.1111/j.1365-246X.2006.03001.x

Momoh, E., Cannat, M., Watremez, L., Leroy, S., Singh, S.C., 2017. Quasi-3-D Seismic Reflection Imaging and Wide-Angle Velocity Structure of Nearly Amagmatic Oceanic Lithosphere at the Ultraslow-Spreading Southwest Indian Ridge. Journal of Geophysical Research: Solid Earth 122, 9511–9533. https://doi.org/10.1002/2017JB014754

Olive, J.A., Behn, M.D., Tucholke, B.E., 2010. The structure of oceanic core complexes controlled by the depth distribution of magmaemplacement. Nature Geoscience 3, 491–495. https://doi.org/10.1038/ngeo888

Oufi, O., Cannat, M., Horen, H., 2002. Magnetic properties of variably serpentinized abyssal peridotites. Journal of Geophysical Research 107, 2095. https://doi.org/10.1029/2001JB000549

Paquet, M., Cannat, M., Brunelli, D., Hamelin, C., Humler, E., 2016. Effect of melt/mantle interactions on MORB chemistry at the easternmost Southwest Indian Ridge (61°–67°E). Geochemistry, Geophysics, Geosystems. https://doi.org/10.1002/2016GC006385

Parnell-Turner, R., Sohn, R.A., Peirce, C., Reston, T.J., MacLeod, C.J., Searle, R.C., Simão, N.M., 2017. Oceanic detachment faults generate compression in extension. Geology 45, 923–926. https://doi.org/10.1130/G39232.1

Patriat, P., Segoufin, J., 1988. Reconstruction of the Central Indian Ocean. Tectonophysics. https://doi.org/10.1016/0040-1951(88)90267-3

Picazo, S., Cannat, M., Delacour, A., Escartín, J., Rouméjon, S., Silantyev, S., 2012. Deformation associated with the denudation of mantle-derived rocks at the Mid-Atlantic Ridge 13°-15°N: The role of magmatic injections and hydrothermal alteration. Geochemistry, Geophysics, Geosystems. https://doi.org/10.1029/2012GC004121

Püthe, C., Gerya, T., 2014. Dependence of mid-ocean ridge morphology on spreading rate in numerical 3-D models. Gondwana Research. https://doi.org/10.1016/j.gr.2013.04.005

Reston, T., 2018. Flipping detachments: The kinematics of ultraslow spreading ridges. Earth and Planetary Science Letters. https://doi.org/10.1016/j.epsl.2018.09.032

Reston, T.J., McDermott, K.G., 2011. Successive detachment faults and mantle unroofing at magma-poor rifted margins. Geology 39, 1071–1074. https://doi.org/10.1130/G32428.1

Reston, T.J., Ranero, C.R., 2012. The 3-D geometry of detachment faulting at mid-ocean ridges. Geochemistry, Geophysics, Geosystems 12, 1–19. https://doi.org/10.1029/2011GC003666

Rouméjon, S., Cannat, M., 2014. Serpentinization of mantle-derived peridotites at mid-ocean ridges: Mesh texture development in the context of tectonic exhumation. Geochemistry, Geophysics, Geosystems. https://doi.org/10.1002/2013GC005148

Rouméjon, S., Cannat, M., Agrinier, P., Godard, M., Andreani, M., 2014. Serpentinization and fluid pathways in tectonically exhumed peridotites from the southwest Indian ridge (62-65°E). Journal of Petrology 56, 703–734. https://doi.org/10.1093/petrology/egv014

Sauter, D., Cannat, M., Rouméjon, S., Andreani, M., Birot, D., Bronner, A., Brunelli, D., Carlut, J., Delacour, A., Guyader, V., MacLeod, C.J., Manatschal, G., Mendel, V., Ménez, B., Pasini, V., Ruellan, E., Searle, R., 2013. Continuous exhumation of mantle-derived rocks at the Southwest Indian Ridge for 11 million years. Nature Geoscience 6, 314–320. https://doi.org/10.1038/ngeo1771

Schlindwein, V., Schmid, F., 2016. Mid-ocean-ridge seismicity reveals extreme types of ocean lithosphere. Nature 535, 276–279. https://doi.org/10.1038/nature18277

Schroeder, T., John, B.E., 2004. Strain localization on an oceanic detachment fault system, Atlantis Massif, 30°N, Mid-Atlantic Ridge. Geochemistry, Geophysics, Geosystems 5. https://doi.org/10.1029/2004GC000728

Smith, D.K., Cann, J.R., 1999. Constructing the upper crust of the Mid-Atlantic Ridge: A reinterpretation based on the Puna Ridge, Kilauea Volcano. Journal of Geophysical Research: Solid Earth 104, 25379–25399. https://doi.org/10.1029/1999JB900177

Smith, D.K., Cann, J.R., Escartín, J., 2006. Widespread active detachment faulting and core complex formation near 13°N on the Mid-Atlantic Ridge. Nature 442, 440–443. https://doi.org/10.1038/nature04950

Standish, J.J., Dick, H.J.B., Michael, P.J., Melson, W.G., O'Hearn, T., 2008. MORB generation beneath the ultraslow spreading Southwest Indian Ridge (9-25°E): Major element chemistry and the importance of process versus source. Geochemistry, Geophysics, Geosystems 9. https://doi.org/10.1029/2008GC001959

Tian, X., Choi, E., 2017. Effects of axially variable diking rates on faulting at slow spreading mid-ocean ridges. Earth and Planetary Science Letters 458, 14–21. https://doi.org/10.1016/j.epsl.2016.10.033

Tucholke, B.E., Behn, M.D., Buck, W.R., Lin, J., 2008. Role of melt supply in oceanic detachment faulting and formation of megamullions. Geology. https://doi.org/10.1130/G24639A.1

Wolfe, C.J., Purdy, G.M., Toomey, D.R., Solomon, S.C., 1995. Microearthquake characteristics and crustal velocity structure at 29°N on the Mid-Atlantic Ridge: The architecture of a slow spreading segment. Journal of Geophysical Research. https://doi.org/10.1029/95JB02399

Yu, Z., Li, J., Niu, X., Rawlinson, N., Wang, W., Hu, H., Wei, X., Zhang, J., Lian, Y., 2018. Lithospheric Structure and Tectonic Processes Constrained by Microearthquake Activity at the Central Ultraslow-. Journal of Geophysical Research : Solid Earth 6247–6262.

Zhao, M., Qiu, X., Li, J., Sauter, D., Ruan, A., Chen, J., Cannat, M., Singh, S., Zhang, J., Wu, Z., Niu, X., 2013. Three-dimensional seismic structure of the Dragon Flag oceanic core complex at the ultraslow spreading Southwest Indian Ridge (49°39'E). Geochemistry, Geophysics, Geosystems 14, 4544–4563. https://doi.org/10.1002/ggge.20264